International Journal of Machine Tools & Manufacture 50 (2010) 824–833

Contents lists available at ScienceDirect

International Journal of Machine Tools & Manufacture

journal homepage: www.elsevier.com/locate/ijmactool

A study on droplets and their distribution for minimum quantity lubrication (MQL)

Kyung-Hee Park [a], Jorge Olortegui-Yume [a], Moon-Chul Yoon [b], Patrick Kwon [a,*]

[a] Department of Mechanical Engineering, Michigan State University, East Lansing, MI, United States
[b] Division of Mechanical Engineering, Pukyong National University, Pusan, Republic of Korea

ARTICLE INFO

Article history:
Received 15 August 2008
Received in revised form
3 May 2010
Accepted 5 May 2010
Available online 31 May 2010

Keywords:
Confocal laser scanning microscopy (CLSM)
MQL droplet size and distribution
Image processing
Wavelet transform

ABSTRACT

A better understanding in the application of minimum quantity lubrication (MQL) or near dry machining (NDM) is needed for its effective use in practical industrial applications. This paper presents the combination of confocal laser scanning microscopy (CLSM) and image processing techniques including wavelet transform to characterize the droplet sizes and the droplet distribution after MQL oil has been sprayed onto a polished silicon wafer. The raw droplet topographies captured with CLSM have been wavelet-filtered to purge the noise and artifacts and then the droplets themselves were isolated using wavelets multi-resolution analysis in order to measure the volume of each droplet. In addition, the empirical droplet size estimation equation was introduced for extremely small droplets which are difficult to measure. The distribution of the droplets has been also studied to determine the MQL optimal nozzle–workpiece distance and the nozzle discharge pressure. The procedures developed in this paper can be used to determine optimal conditions for various applications of MQL processes.

1. Introduction

In modern metal cutting applications, the cutting temperatures and forces on a cutting tool are typically high, which drastically reduces tool life. For this reason, the cutting zone must be well lubricated and adequately cooled by applying coolants in most machining applications. For optimal machining operations, the coolants must be maintained throughout their usage and eventually disposed. Recently, minimum quantity lubrication (MQL) or near dry machining (NDM) has been applied to reduce the cost associated with the maintenance and disposal of the sheer volume of fluid being used and the conformation to environmental policies [1–3]. In MQL, the high pressurized air sprays micro-scale lubricant droplets onto the tool–work interface. Even though it is very promising for many machining applications [3–5], several fundamental issues associated with MQL such as optimal conditions for the operations and environmental concerns have not been fully addressed [6].

Typical oil-based lubricants used in MQL do not have the heat capacity of water-based coolants. Accordingly, the most important function provided by the lubricants in MQL is to reduce the friction between tool and work material. Thus, the most important point in the MQL process is that the lubricant must adequately cover the contact areas, i.e., tool–chip and tool–work interfaces. Particularly, droplet size and distribution in terms of nozzle distance and air pressure have to be considered because the smaller droplet, which can provide better penetration into the cutting surface, are more preferable especially for micro-machining applications where the cutting surface is relatively small [7]. In addition, droplet distribution, which associated with the wetting area by lubricant, can affect the cutting performance as well. Other important variables are wettability on the tool surface [6] and thermal–chemical stability of lubricant. For example, vegetable oil shows poor stability against oxidation and thermal degradation while mineral oil has important health related issues as will be discussed later. In this regard, several works have been reported not only for improvement of the thermal–chemical stability by additives or chemical modification of the vegetable oil but for optimal lubricants in MQL application [8–11]. Thus far, the efforts for understanding of these MQL parameters have not been considerably made. Therefore, a better understanding of the MQL application conditions such as droplet size and distribution, air pressure, nozzle distance, and flow rate is needed prior to machining process in industrial applications.

The operator's health hazards have been a major concern whenever lubricants/coolants are used in machining operations. For instance, in flood cooling, the workers are exposed with a variety of respiratory disorders including occupational asthma, hypersensitive pneumonia and loss of lung function and skin disease such as irritation, oil acne and skin cancer [12]. The major

* Corresponding author.
E-mail addresses: parkkyu5@msu.edu (K.-H. Park), olortegu@egr.msu.edu (J. Olortegui-Yume), mcyoon@pknu.ac.kr (M.-C. Yoon), pkwon@egr.msu.edu (P. Kwon).

0890-6955/$ - see front matter © 2010 Elsevier Ltd. All rights reserved.
doi:10.1016/j.ijmachtools.2010.05.001

industrial concern for MQL is the use of very fine, airborne fluid droplets which potentially pose a potential health risk for machine operators. This can be circumvented by installing the vacuum system in tandem with the MQL sprayer. However, the extent of health hazards depends on the concentration and the type of lubrication fluid used (mineral, vegetable or animal, water soluble and semi- or synthetic) as well as the duration of exposure. The characteristics such as mist droplets diameter and mass concentration generated are varied depending on the type of oils [13]. Mineral oil may cause more serious damage to human body than vegetable oil. Mineral (petroleum-based) oil is retained in the lung and cause lung fibroses while vegetable oil is eliminated from the lung within a few days without any obvious damage to the lung [14,15]. With the droplet (mist) size less than 4 μm, even MQL can cause various occupational diseases. In fact it was reported to deteriorate lung function even for short-term exposure [13]. Therefore, the National Institute for Occupational Safety and Health (NIOSH) has recommended that the exposure to metal working fluid mist is limited to 0.5 mg/m^3 for total particulate mass as the recommended exposure limit (REL) [16]. Thus, a great interest exists in the machining community in the development of a convenient technique to measure the droplet sizes in terms of lubricant types and spray conditions.

To address various issues mentioned above, confocal laser scanning microscopy (CLSM) is used for the first time for this purpose. CLSM is an established advanced microscopy technique used in a variety of fields to obtain accurate surface topography [17]. In particular, CLSM can be successfully applied to characterize the crater wear of cutting tools [18]. Wavelet transform can be useful when the dynamic or localized properties of surfaces are needed as opposed to the fixed wavelength harmonics assumed by classical Fourier transform (FT) or Gabor transform [19,20]. When wavelets are applied in cascade to the surface data, a multi-resolution representation of the surface can be obtained, i.e. surface representations at multiple scales [21]. The availability of the wavelet representations facilitates the researcher to perform tasks such as data de-nosing and identification of roughness features.

In this paper, we have developed a new technique to measure the droplet sizes in a typical MQL process and their distribution after the droplets have been sprayed onto the polished silicon wafer surface. CLSM has been utilized for three-dimensional (3D) surface characterization of the droplet surface for the droplet volume measurement. The raw data from CLSM contains noise and artifacts due to the inherent nature of data acquisition process. To circumvent these problems, wavelets analysis has been applied by the use of de-noising schemes and multi-resolution decomposition which helps to extract the droplet profile. In addition, edge detection algorithm (EDA) has been used to obtain the droplet distribution in terms of nozzle distances and air pressures. These developments have been used to study the effects of air pressure on the droplet size and distribution.

2. Experimental set-up

Sharnoa SVC-60 CNC milling machine was used to provide the movement for the silicon wafer mounted on the CNC table while the MQL dispensing unit (Unimax-Part no. 9570-7-5-12- UNIST) equipped with a flexible nozzle was used to spray vegetable oil-based lubricant (UNIST-Coolube 2210). The MQL droplets were sprayed onto a silicon wafer to minimize the surface roughness in order to accommodate the task of extracting the droplet shape in the wavelets analysis. The set-up for MQL spray experiment is shown in Fig. 1. The droplets discharged from the nozzle with the flow rate of 3.2 ml/min, which was measured by detecting the loss

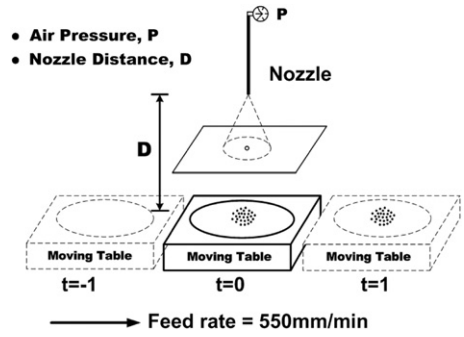

Fig. 1. MQL experimental set-up.

in the oil height through a graduated thin glass cylinder, are passed through the screening plate with a hole in order to block most of the oil mist stream and thus avoid droplet overlap on the wafer. After trying various hole diameters, it was set at 0.8 mm because the droplet size did not decrease any further below this value. The droplets were discharged as a function of air pressure, P, and nozzle distance, D, in order to investigate their influence over the droplet size and distribution. To evaluate the effect of air pressure, mass accumulation test was developed, where an absorbent sheet placed on a wax paper was placed on the polished silicon wafer. With the mass accumulation test, the oil droplets that are eventually attached to the silicon wafer can be distinguished from the airborne droplets. This test was performed in terms of air pressure and nozzle distance. Similarly, the sprayed droplets from the nozzle were absorbed into the mass measuring paper at the pressure of 4 and 8 psi at the flow rate of 3.2 ml/min.

3. CLSM data acquisition and image processing

The important characteristic of CLSM is the confocal aperture which eliminates the reflected light from above and below the focal plane, thus obtaining surface information from a very thin "optical slice" of the surface is feasible. Surface reconstruction is achieved by storing and manipulating a stack of optical slices within a set of the vertical travel of the stage. The final output of the built-in software in CLSM is a z-matrix ($z(x,y)$) containing the height information of the surface. For a better handling of the image data, the z-matrix is encoded in a grayscale, called height encoded image (HEI). Along with HEIs, maximum brightness images (MBIs), which are extended depth of field views, can be also obtained. It is important to note that most confocal systems can work in both confocal and optical (conventional) modes. The detail information on CSLM can be found in [17,18]. In this work, a Zeiss LSM210 confocal system was used to capture 2D images (confocal slices) and HEIs (topography) of individual droplets using Plan Neofluar 5 × /0.15 and 50 × /0.80 objectives. Fig. 2(a) and (b) shows the 2D CLSM droplet images at 4 and 8 psi, respectively, obtained with the 5 × /0.15 objective. These images are used for identifying the droplet size distribution and the droplet coverage area fraction deposited on the wafer. The boundaries of each droplet were detected using EDA called 'Canny' which looks for local maxima of the intensity gradient in an image. Then the areas enclosed by detected boundaries were filled and considered as the sprayed droplets as shown in Fig. 2(c) and (d). It was assumed that the areas smaller than 2 pixels (1 pixel = 5.87265 × 4.16792 μm/5 × objective) were rejected. On the other hand, for droplet size measurement, HEIs were obtained for various sizes of individual droplets, as shown in Fig. 3.

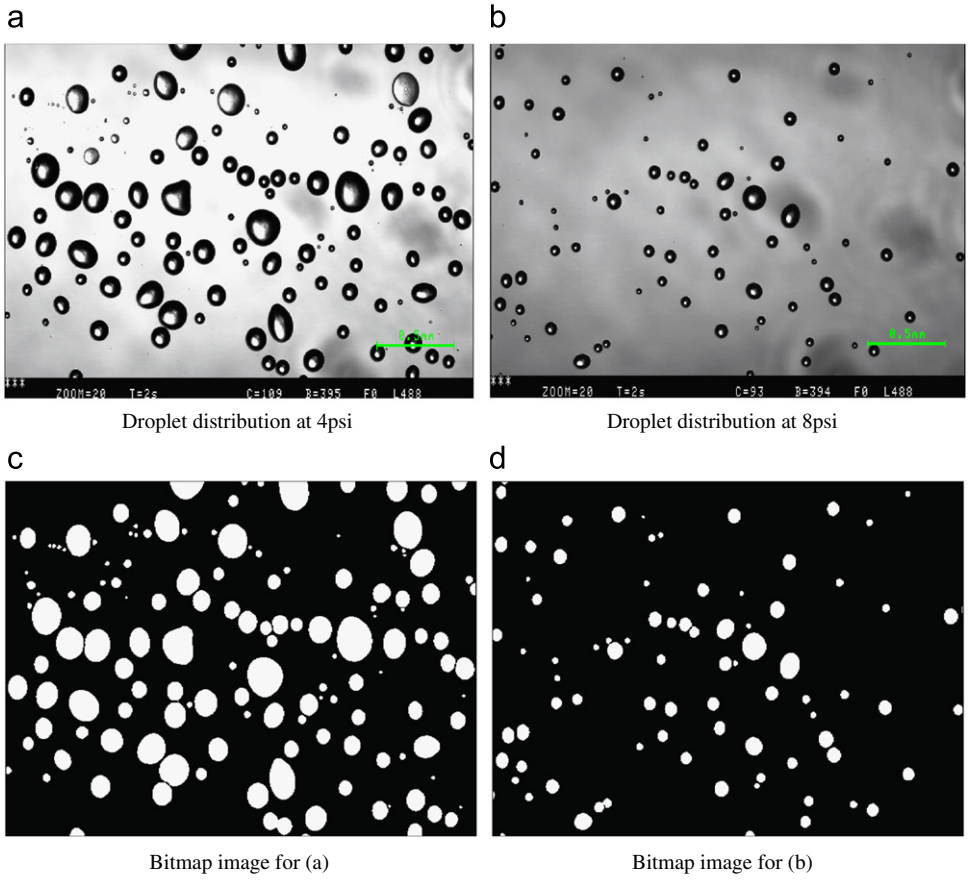

Fig. 2. Droplets distribution optical images from confocal microscope and bitmap images obtained by EDA at 4 and 8 psi.

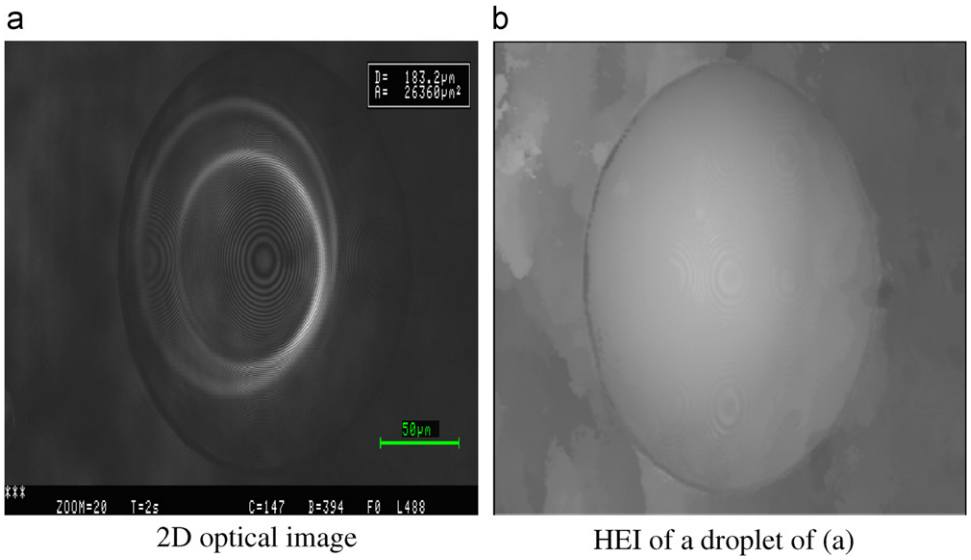

Fig. 3. Droplet images for droplet size measurement.

The main advantage of the wavelet transform for image processing is to extract the surface topography clearly from the raw image data without loosing any surface details [22,23]. In this work, the two-dimensional discrete wavelet transform (2D-DWT) was used in a multi-resolution scheme with a two-channel filter bank, which consists of a pair of filters, low-pass and high-pass filters based on a chosen mother wavelets, Daubechies7 (db7) [20]. For acquisition of the droplet topography (3D), the wavelet de-noising was required to eliminate the electronic noise and artifacts from individual droplet images (HEIs). The de-noised surface topography data was then post-processed using multi-resolution wavelets analysis. Finally, the droplet size can be obtained by calculating the droplet volume (see Section 4).

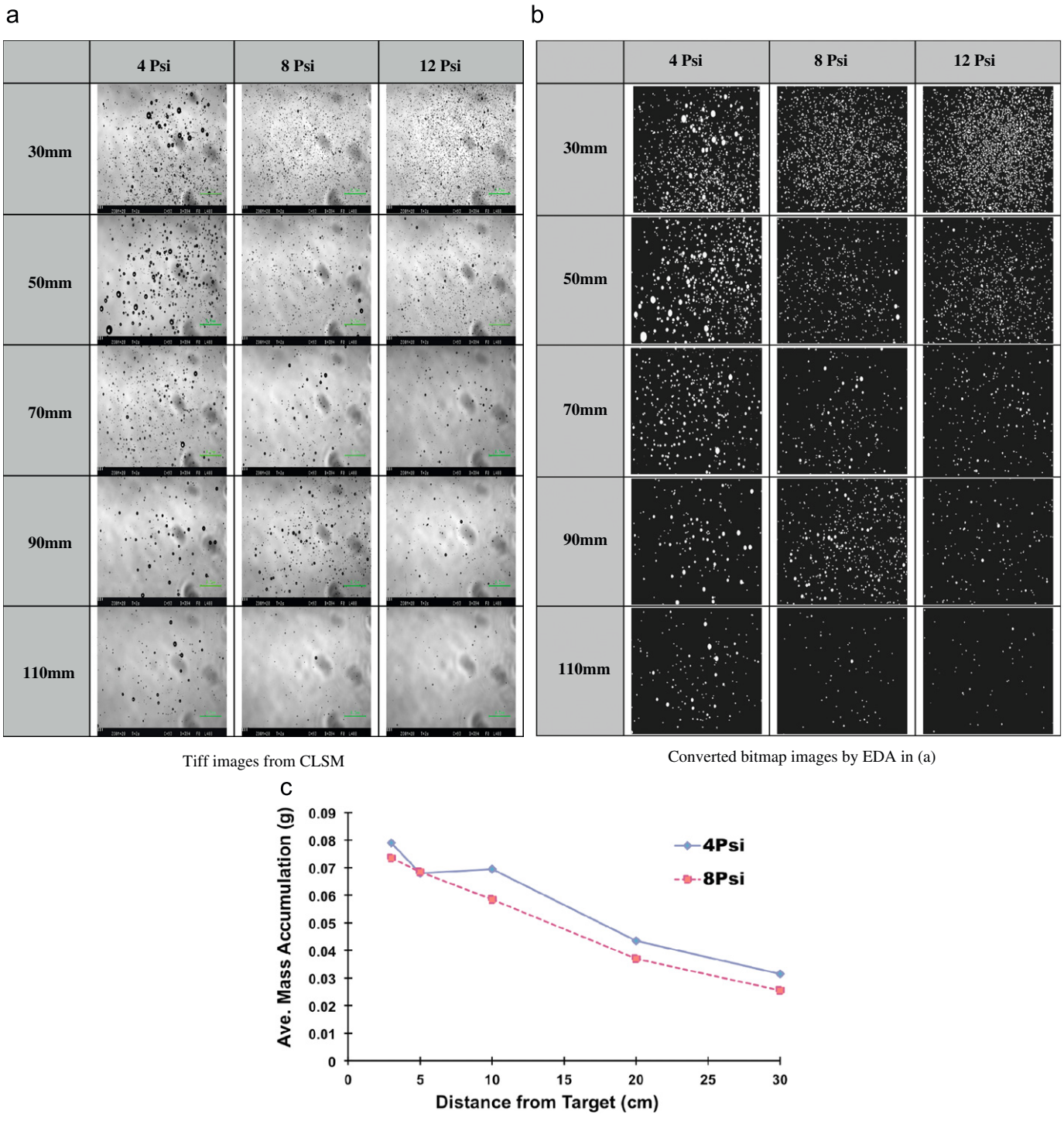

Fig. 4. The sprayed confocal images (a), corresponding bitmap images (b), and average mass accumulation (c) in terms of the nozzle distance and air pressure.

Table 1
Average sizes, droplet count, and area fractions.

Nozzle distance (mm)	**Nozzle air pressure (psi)**								
	4			**8**			**12**		
	D_{av} (μm)	N_d	A_f (%)	D_{av} (μm)	N_d	A_f (%)	D_{av} (μm)	N_d	A_f (%)
30	12.93	888	9.3	11.28	1335	9.6	11.32	2066	15.1
50	15.18	595	8.9	12.66	471	4.5	10.54	797	5.0
70	13.94	362	4.5	12.29	217	2.0	11.85	217	1.7
90	15.47	151	2.4	11.05	485	3.4	11.70	160	1.2
110	13.32	144	1.6	11.04	71	0.5	10.15	58	0.3

A_f: area fraction covered by droplets (%); N_d: droplet count; D_{av}: average diameter (μm).

4. Droplet volume calculation

Once the droplets are deposited onto the flat silicon wafer surface, each droplet spreads and changes its morphology while preserving the volume of each droplet. Using the HEI information, the volume of droplet can be calculated as follows:

$$V_{droplet} = \Sigma \Delta V_{i,j} = \sum_{i=1}^{M} \sum_{j=1}^{N} \Delta x \Delta y (h_{i,j} - h_{zero}) \quad (1)$$

where $\Delta V_{i,j}$ is the discrete volume at a point $P_{i,j}(x_i, y_j, z_{i,j})$, $h_{i,j}$ is the surface height of droplet at a point $P_{i,j}$ and h_{zero} is considered as the height of the droplet edge. The total volume of a droplet can be obtained by summing up the discrete volume, $\Delta V_{i,j}$. The height $z_{i,j}$ is obtained as a result of HEI decoding. M and N correspond to the size of the HEI. Once the droplet volume is calculated, the diameter of a spherical airborne droplet, D_{eq}, can be defined as

$$D_{eq} = 2\left[\frac{3V_{droplet}}{4\pi}\right]^{1/3} \quad (2)$$

5. Results and discussion

5.1. Droplet size and distribution

The 2D CLSM images of sprayed droplets obtained under various operating conditions (Fig. 4(a)) were converted into their bitmap versions (Fig. 4(b)), which were ultimately used to calculate the average sizes of droplets as well as the area fraction covered by droplets. Table 1 summarizes the quantitative results of these calculations. It was observed that, as the nozzle distance increased, the surface area covered by the droplets decreased. The spray conditions for the maximum surface coverage were observed at a nozzle distance of 30 mm and air pressure of 12 psi. This is because more droplets are released from the nozzle within a unit time and thus more of them can cross the screening plate at a higher air pressure. However, the area fraction decreased substantially at the nozzle pressure of 12 psi as the nozzle distance increased. For example, as seen in Table 1, at the air pressure of 12 psi, the covered area fraction dropped from 15.1% at the nozzle distance of 30 mm to 1.7% at that of 70 mm. The reduction of the area fraction is more substantial at a higher air pressure.

The droplet size at higher pressure is smaller than that of lower pressure. In addition, Fig. 4(c) shows air pressure effect on the oil mass accumulation test. After the oil was sprayed in terms of the nozzle distance and air pressure, the oil mass accumulated on the absorbent paper was measured. The average mass accumulated decreased as the nozzle distance and the air pressure increased as shown in Fig. 4(c). Moreover, the oil mass could not be measured at a higher air pressure because the spray was too vigorous so that the oil mist cloud was generated in the air rather than accumulated on the absorbent paper. Thus, accurate data could not be obtained at higher air pressure. Based on mass accumulation test, the short nozzle distance is more preferable and too high air pressure might not wet the cutting surface effectively, especially with the increase in the nozzle distance if the small cutting zone is considered. Therefore, it can be concluded that the nozzle distance should be less than 50 mm and if the high air pressure is required, the nozzle distance should be short enough to provide adequate lubricant at the cutting zone.

5.2. Droplet volume calculation by wavelet transformation

The general procedure used to calculate the droplet size includes the CLSM data acquisition, the wavelets de-noising step, the wavelets multi-resolution analysis, and the droplet volume calculation as presented in Fig. 5. In addition, an empirical model is developed to estimate the droplet diameters sprayed in the air based on the relationship between 2D CSLM images and 3D HEIs (see Section 4.4).

Fig. 6(a) shows the raw HEI of an individual droplet obtained at the compress air pressure of 6 psi and the nozzle distance of 55 mm using the 50 × /0.80 objective in the CLSM. Each pixel size for the 50 × objective is 1.14745 × 0.764706 μm. In the HEI (Fig. 6(a)), the surface height at a position (x,y) is encoded such that the bright pixels indicate high positions relative to dark pixels. For more accurate calculation, only droplet surface area was cropped using image processing software as shown in Fig. 6(a). Fig. 6(b) shows the 3D surface reconstruction of the droplet surface using the raw HEI in Fig. 6(a). The droplet HEI was post-processed using a wavelet-de-noising algorithm (Daubechies) to filter out electronic noise and unusual pits/peaks (artifacts) present. This de-noised HEI was used as an input for the multi-resolution analysis up to level 7 using Daubechies7 (db7) mother wavelet. After inspecting the decoupled approximation and detail surfaces, a threshold level was defined beyond which distortion impairs the useful extraction of the droplet shape. Raw HEIs contain the topography of the surface mixed with noise and artifacts. However, even if all the noise and artifacts are eliminated, the remaining information in the HEIs could contain the tilting of the silicon wafer stages and of the substrates (wafers in this case). Extracting the droplet shape from a tilted surface is considerably difficult; thus, tilting was compensated using mean slope obtained by the average of the slopes in both x and y directions both tilted shapes are shown in Fig. 6(b) and (c). The slope compensation is carried out after wavelet multi-resolution analysis and prior to the droplet volume calculation.

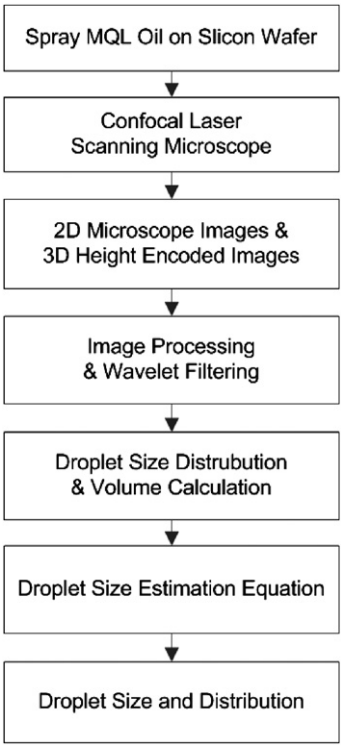

Fig. 5. Flow chart for the calculation of the droplet size and distribution.

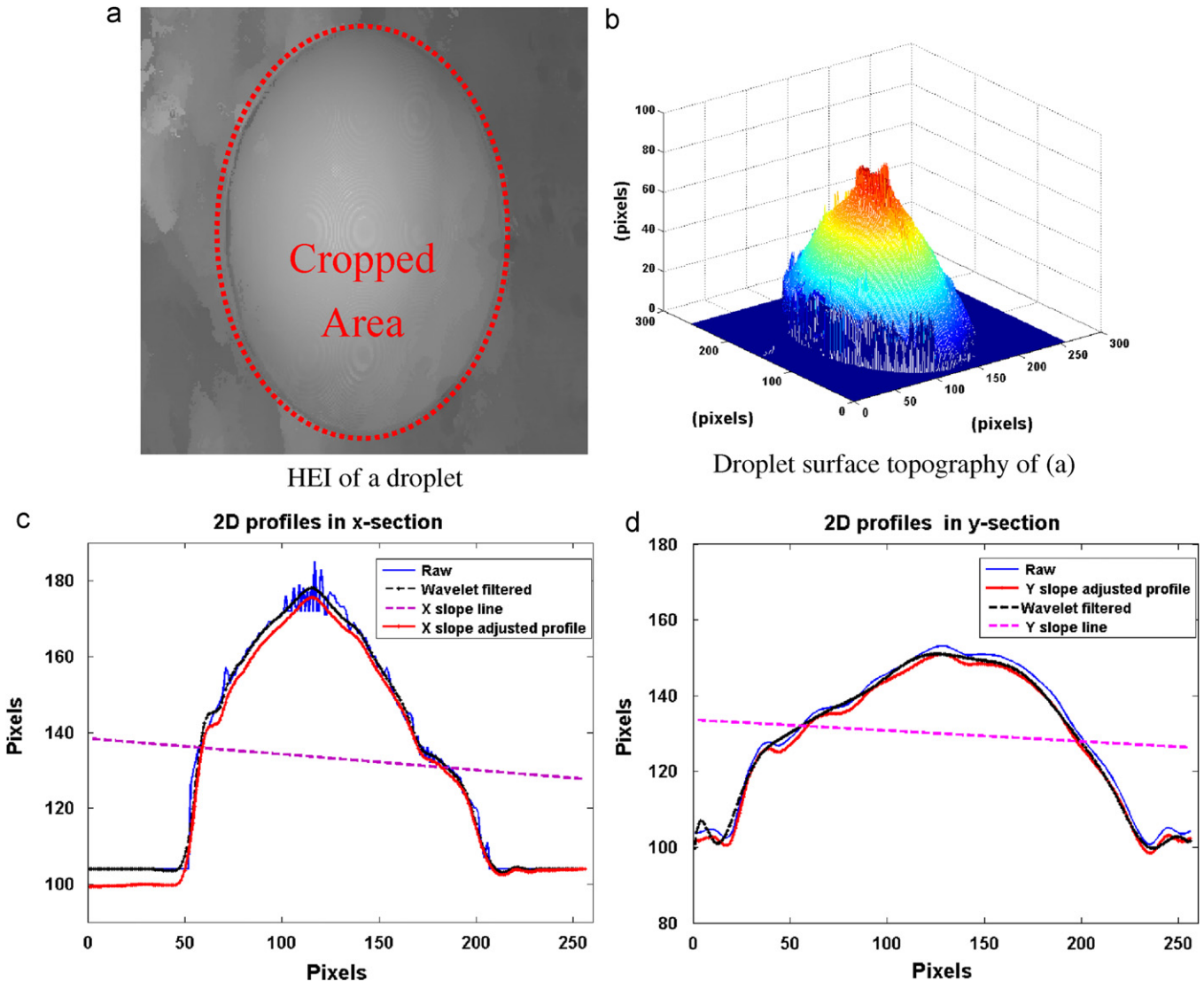

Fig. 6. HEI image of the droplet (a), 3D surface profile (b) and 2D droplet profiles in *x* (c) and *y* section (d) at level 3.

Fig. 7 presents the approximations and details surfaces (horizontal, vertical and diagonal) obtained up to 7th level after applying the wavelet transform including the reconstruction (inverse transformation) process. It can be clearly observed that between levels 1 through 4 (Fig. 7(b)) the decoupling of the droplet (large features) from the details (small features) is consistent with our purpose. In other words, the approximation surface contains mainly the dominant shape (the droplet) while the detail surfaces contain much smaller features. In this study, only the approximations were used for the droplet profiles and volume calculations since the small features such as roughness and waviness were of no interest. After the 4th level of decomposition, this behavior is no longer observed and between levels 5th and 7th larger features are being extracted implying a major distortion in the droplet shape.

Fig. 8 shows the approximation droplet surfaces for all levels up to the 6th level of wavelet decomposition. It is clearly observed that the 4th level is the threshold limiting the feasible extraction of the droplet shape. Thus, the images between 1st and 4th levels with the droplet pattern clearly were used for the volume calculation.

Using the droplet surface of Fig. 8(c), the estimation of droplet volume was conducted. The total calculated droplet volume using Eq. (1) at level 3 is $2.1084E-004\,mm^3$. The droplet volume calculated in each level can be shown as in Fig. 9(b). The calculated droplet volumes from 1st to 7th level of wavelet decomposition are similar, but it shows a large deviation above 7th level. With this droplet volume calculation technique, further analysis with other droplet details such as wetting angle and average droplet size, can be conducted for various commercial lubricants. In this sense, the equivalent droplet radius is estimated at level 3 as 36.92 μm using Eq. (2) and the equivalent droplet radius in several levels can be shown as Fig. 9(c). It shows the similar trend with droplet volume at each level. As shown in Fig. 9(b) and (c), the droplet surface profiles were completely lost at 8th level.

5.3. Small droplet size estimation

The capturing of HEIs (3D data) for very small droplets with the average diameter, $D_{av} < 100$ μm, can be challenging and time consuming. Thus, an estimation method was pursued. A diameter estimation equation for a spherical airborne droplet (3D) can be achieved by using the CLSM optical image (2D version) and the calculated volume of a droplet (3D). For example, both the optical and HEIs for the droplets are taken by CLSM. Using volume calculation method in Section 4.3 and Eq. (2), 3D diameters of

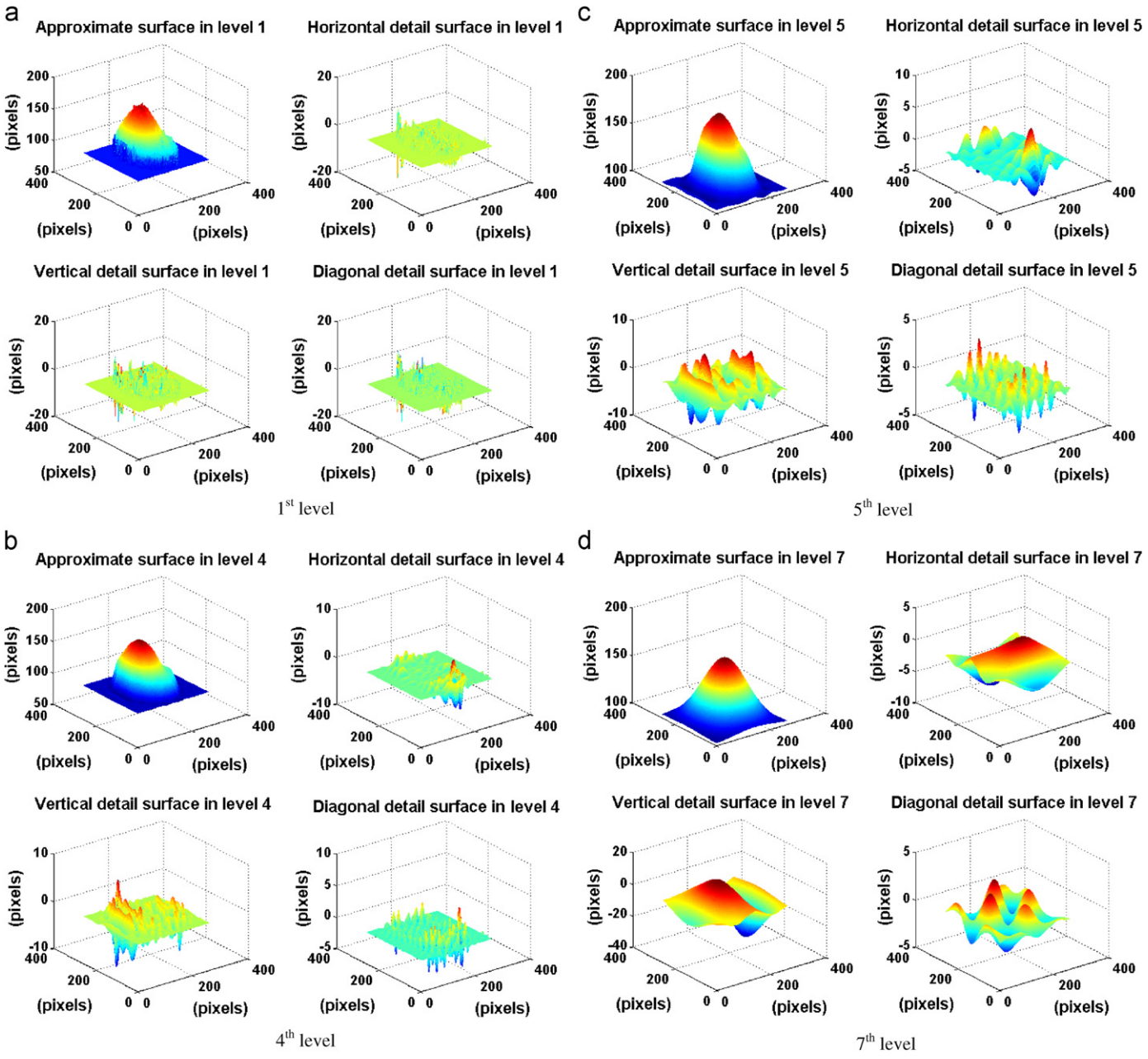

Fig. 7. The droplet surfaces after wavelet transform.

airborne droplets can be obtained. Fig. 10(b) and (d) represent the droplet volumes calculated by wavelet-transform for different droplet sizes and Fig. 10(a) and (c) are their corresponding 2D droplet images, respectively. In addition, for the small droplet estimation, relationship between 2D and 3D droplet diameters was determined by using interpolation method as follows:

$$D_{3D} = 0.0012D_{2D}^2 + 0.1997D_{2D} - 0.0987 \quad (3)$$

where D_{2D} is the 2D diameter of a droplet on the silicon wafer and D_{3D} is the diameter of an airborne droplet. This empirical correlation between the diameters in the 2D images and the diameters in the 3D data (HEIs) should be limited to the combination of the lubricant and the silicon wafer surface used in this study. To justify the use of this equation, other combination of lubricant and surface need to be studied. Finally, 2D and 3D droplet diameters for various sizes of the droplets for the vegetable oil can be obtained as summarized in Table 2. Finally, without measuring the extremely small droplets, the size of oil droplet sphere sprayed from the nozzle can be estimated. Using Eq. (3), the size distribution of droplets in Fig. 3(a), 3D images, was analyzed and the average 3D droplet size was around 10 μm. Besides, the most of the droplet sizes in this test is less than 20 μm, which might be small enough to be effective in practical MQL application, as shown in Table 3. The proposed method of measuring the droplet size is particularly useful to evaluate the very small droplet sizes if the inhaling of MQL droplets by operators is harmful.

6. Conclusion

The following conclusions can be drawn from the present work:

- The important MQL parameters such as droplet size and distribution were studied in terms of the nozzle distance and air pressure.

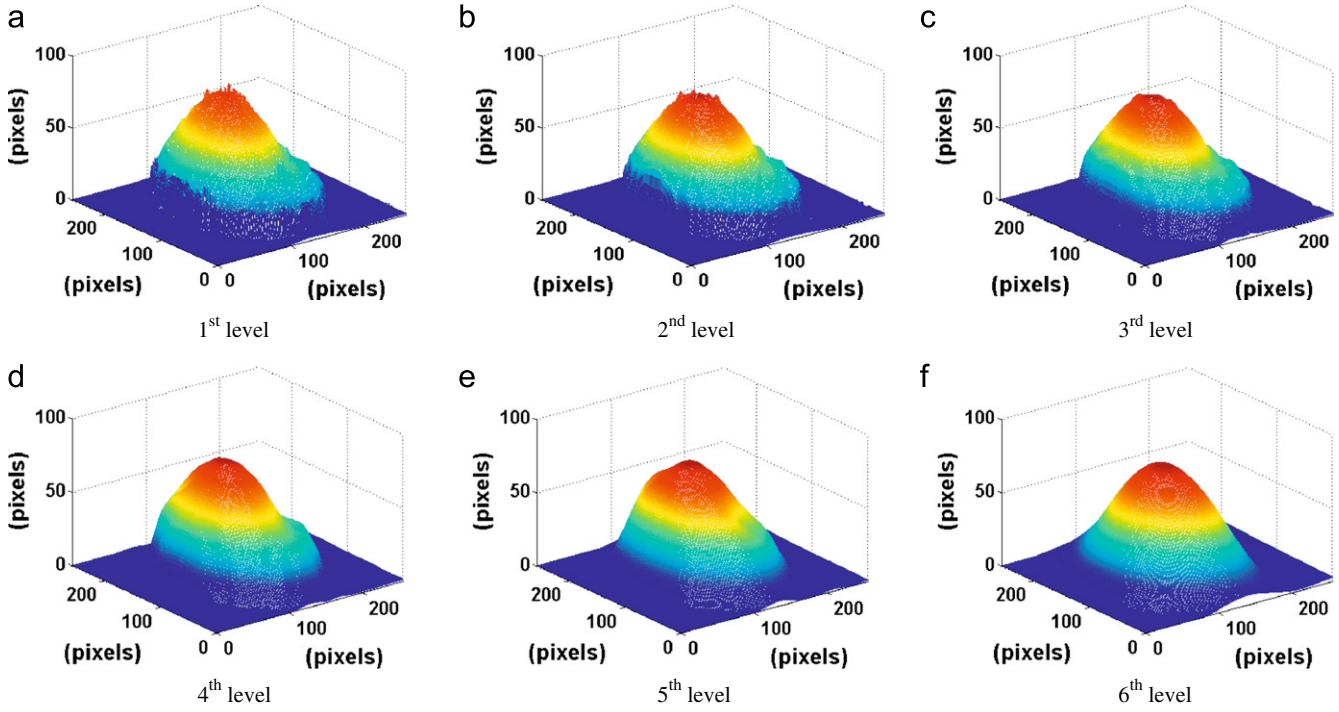

Fig. 8. Droplet surface after wavelet transform in 1st to 6th level.

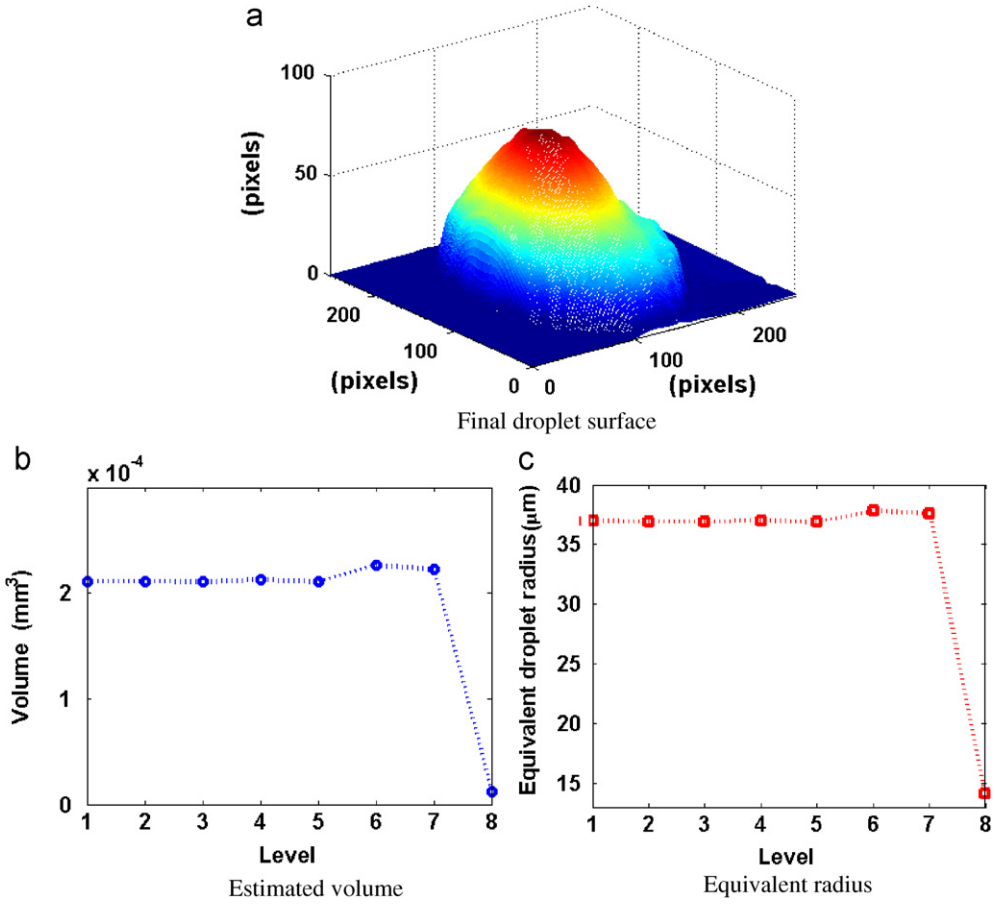

Fig. 9. Droplet surface at level 3 (a) and its corresponding estimated droplet volume (b) and equivalent radius (c).

- The experimental technique to measure the droplet sizes and distribution for MQL combining CSLM and wavelets analysis proposed and proved to be successful.
- Using the edge detection algorithm, the boundary of each droplet on the substrate was identified and the area fraction covered by the droplets based on the area and average size

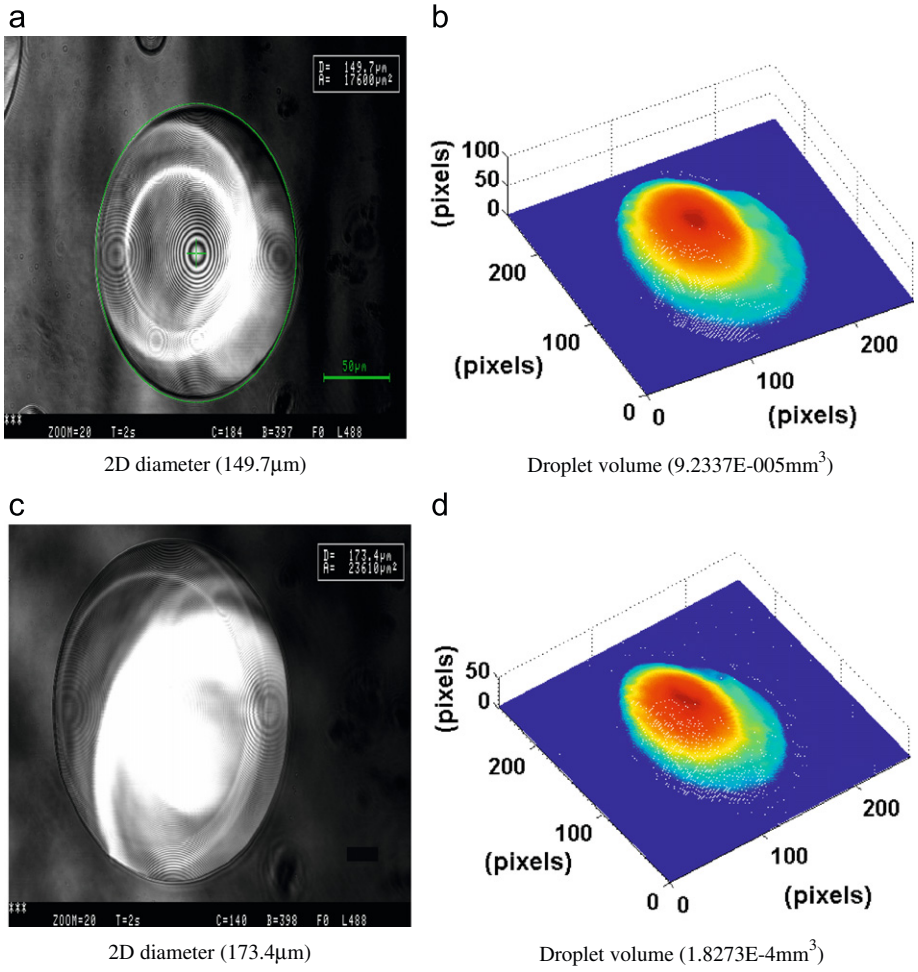

2D diameter (149.7μm) Droplet volume (9.2337E-005mm^3)

2D diameter (173.4μm) Droplet volume (1.8273E-4mm^3)

Fig. 10. Droplet volumes corresponding 2D droplet sizes.

Table 2
Droplet size calculation.

	2D droplet diameter (μm)	3D droplet diameter (μm)
0	0	0
1	96.1	29.2
2	149.7	56
3	173.4	70.4
4	183.2	73.8

Table 3
Droplet size distribution.

Diameter	Number of droplets (2D) ave. size (43.78 μm)	Number of droplets (3D) ave. size (10.02 μm)
$D < 20$ μm	9	123
20 μm $\leq D < 40$ μm	30	17
40 μm $\leq D < 60$ μm	14	1
60 μm $\leq D < 80$ μm	12	0
80 μm $\leq D < 100$ μm	21	0
100 μm $\leq D$	17	0

(diameter) of droplets can be determined for various nozzle–workpiece distance and nozzle air pressure.

- Based on the observation, it can be inferred that the higher nozzle pressure provided the more droplets but the smaller droplets were obtained while a smaller amount of droplets was deposited on the surface when the nozzle distance was increased. The maximum area fraction covered by droplets was obtained at the nozzle distance of 30 mm and the air pressure of 12 psi. However, high air pressure does not provide the condition to wet the cutting zone especially with the nozzle distance more than 50 mm.
- The volume of a droplet was calculated using wavelet transform (Daubechies7 mother wavelet). The wavelet decomposition of the droplet surfaces was performed up to 7th level and the 4th level is the threshold limit for the feasible extraction of the droplet shape. Therefore, the images between 1st and 4th levels can be used for the volume calculation.
- The size of small droplets (less than 100 μm) can be estimated by using the equation that represents an empirical correlation between diameter of 2D optical droplet images and 3D droplet images. The average diameter of 3D droplets was 10.02 μm. This droplet size information in terms of lubricant type and spray condition can be useful not only to evaluate the penetration ability of lubricant into cutting zone but to determine the operator's health hazards, especially for very small droplets.
- The proposed approach of the MQL parameters in this work can be used to determine optimal MQL conditions prior to each machining application, which ultimately increases the efficiency of the machining process. The optimal MQL parameters will be depending on the particular MQL oil used and an operating condition of a particular MQL system. Thus, this paper introduces a new method for such parametric study.

Acknowledgement

This work was performed at Michigan State University where Prof. M.C. Moon was visiting during his sabbatical from Pukyung National University between 2008 and 2009.

References

[1] K. Weinert, I. Inasaki, J.W. Sutherland, T. Wakabayashi, Dry machining and minimum quantity lubrication, CIRP Annals 53 (2004) 511–537.
[2] T. Ueda, A. Hosokawa, K. Yamada, Effect of oil mist on tool temperature in cutting, Journal of Manufacturing Science and Engineering 128 (2006) 130–135.
[3] M. Rahman, A.S. Kumar, M.U. Salam, Experimental evaluation on the effect of minimal quantities of lubricant in milling, International Journal of Machine Tools and Manufacture 42 (2002) 539–547.
[4] A.S. Varadarajan, P.K. Philip, B. Ramamoorthy, Investigations on hard turning with minimal cutting fluid application (HTMF) and its comparison with dry and wet turning, International Journal of Machine Tools and Manufacture 42 (2002) 193–200.
[5] V.S. Sharma, M. Dogra, N.M. Suri, Cooling techniques for improved productivity in turning, International Journal of Machine Tools and Manufacture 49 (2009) 435–453.
[6] K.-H. Park, J. Olortegui-Yume, S. Joshi, P. Kwon, M.-C. Yoon, G.-B. Lee, S.-B. Park, Measurement of droplet size and volumes for minimum quantity lubrication (MQL), in: International Conference on Smart Manufacturing Application, Gyeonggi-do, Korea, 2008.
[7] M.B.G. Jun, S.S. Joshi, R.E. DeVor, S.G. Kapoor, An experimental evaluation of an atomization-based cutting fluid application system for micromachining, Journal of Manufacturing Science and Engineering 130 (2008) 031118.
[8] B.K. Sharma, A. Adhvaryu, S.Z. Erhan, Friction and wear behavior of thioether hydroxyl vegetable oil, Tribology International 42 (2009) 353–358.
[9] N.J. Fox, G.W. Stachowiak, Vegetable oil-based lubricants—a review of oxidation, Tribology International 40 (2007) 1035–1046.
[10] S. Suda, H. Yokota, I. Inasaki, T. Wakabayashi, A synthetic ester as an optimal cutting fluid for minimal quantity lubrication machining, CIRP Annals 51 (2002) 95–98.
[11] F. Itoigawa, T.H.C. Childs, T. Nakamura, W. Belluco, Effects and mechanisms in minimal quantity lubrication machining of an aluminum alloy, Wear 260 (2006) 339–344.
[12] P.C. Raynor, S.W. Kim, M. Bhattacharya, Mist generation from metalworking fluids formulated using vegetable oils, Annals of Occupational Hygiene 49 (2005) 283–293.
[13] J. Thornburg, D. Lieth, Size distribution of mist generated during metal machining, Applied Occupational and Environmental Hygiene 15 (2000) 618–628.
[14] H. Pinkerton, The reaction to oils and fats in the lung, Archives of Pathology 5 (1928) 380–401.
[15] M. Shoskes, W.G. Banfield, S.J. Rosenbaum, Effect and fate of oil aerosol particles retained in the lungs of mice, A.M.A. Archives of Industrial Hygiene and Occupational Medicine 1 (1950) 20–35.
[16] National Institute for Occupational Safety and Health (NIOSH), Recommendation for a metalworking fluids standard, http://www.cdc.gov/NIOSH/ (Chapter 1).
[17] D.N. Hanlon, I. Todd, E. Peekstok, W.M. Rainforth, S. van der Zwaag, The application of laser scanning confocal microscopy to tribological research, Wear 251 (2001) 1159–1168.
[18] J.A. Olortegui-Yume, P. Kwon, Crater wear evolution in multilayer coated carbides during machining using confocal microscopy, Journal of Manufacturing Processes 9/1 (2007) 47–60.
[19] A. Maksumov, R. Vidu, A. Palazoglu, P. Stroeve, Enhanced feature analysis using wavelets for scanning probe microscopy images of surfaces, Journal of Colloid and Interface Science 272 (2004) 365–377.
[20] O. Rioul, M. Vetterli, Wavelet and signal processing, Signal Processing Magazine IEEE 8 (1991) 14–38.
[21] S. Fu, B. Muralikrishnan, J. Raja, Engineering surface analysis with different wavelet bases, Journal of manufacturing Science and Technology 125 (2003) 844–852.
[22] K.-H. Park, P.Y. Kwon, Flank wear of multi-layer coated tool and wear prediction using abrasive wear model, in: Proceedings of the 2009 AMSE International Manufacturing Science and Engineering Conference, West Lafayette, India, USA.
[23] J.A. Olortegui-Yume, P.Y. Kwon, Crater wear patterns analysis on multi-layer coated carbides using wavelet transform, Wear 268 (2010) 493–504.